Applied Physics Letters

ScAlN/3C-SiC/Si platform for monolithic integration of highly sensitive piezoelectric and piezoresistive devices

Cite as: Appl. Phys. Lett. **116**, 132902 (2020); https://doi.org/10.1063/5.0004943
Submitted: 17 February 2020 . Accepted: 21 March 2020 . Published Online: 01 April 2020

Afzaal Qamar, Hoang-Phuong Phan, Toan Dinh, Nam-Trung Nguyen, and Mina Rais-Zadeh

Applied Physics Letters ARTICLE scitation.org/journal/apl

ScAlN/3C-SiC/Si platform for monolithic integration of highly sensitive piezoelectric and piezoresistive devices

Cite as: Appl. Phys. Lett. **116**, 132902 (2020); doi: 10.1063/5.0004943
Submitted: 17 February 2020 · Accepted: 21 March 2020 ·
Published Online: 1 April 2020

Afzaal Qamar,[1,a)] Hoang-Phuong Phan,[2] Toan Dinh,[3] Nam-Trung Nguyen,[2] and Mina Rais-Zadeh[1,4]

AFFILIATIONS

[1]Department of Electrical Engineering and Computer Science, University of Michigan, Ann Arbor, Michigan 48109, USA
[2]Queensland Micro- and Nanotechnology Centre, Griffith University, Queensland 4111, Australia
[3]School of Mechanical and Electrical Engineering, University of Southern, Queensland 4350, Australia
[4]NASA Jet Propulsion Laboratory, California Institute of Technology, Pasadena, California 91109, USA

[a)]Author to whom correspondence should be addressed: afzaal@umich.edu

ABSTRACT

This paper reports on a platform for monolithic integration of piezoelectric and piezoresistive devices on a single chip using the ScAlN/3C-SiC/Si heterostructure. Surface acoustic wave devices with an electromechanical coupling of 3.2% and an out-of-band rejection as high as 18 dB are demonstrated using the excellent piezoelectric properties of ScAlN and low acoustic loss of 3C-SiC. Additionally, a large piezoresistive effect in the low-doped n-type 3C-SiC(100) thin film has been observed, which exceeds the previously reported values in any SiC thin films. The growth of the n-type 3C-SiC thin film was performed using the low pressure chemical vapor deposition technique at 1250 °C and the standard micro-electro-mechanical systems process is used for the fabrication of 3C-SiC piezoresistors. The piezoresistive effect was measured using the bending beam method in different crystallographic orientations. The maximum gauge factor is –47 for the longitudinal [100] orientation. Using the longitudinal and transverse gauge factors for different crystallographic orientations, the fundamental piezoresistive coefficients of the low-doped n-type 3C-SiC thin film are measured to be $\pi_{11} = (-14.5 \pm 1.3) \times 10^{-11}$ Pa^{-1}, $\pi_{12} = (5.5 \pm 0.5) \times 10^{-11}$ Pa^{-1}, and $\pi_{44} = (-1.7 \pm 0.7) \times 10^{-11}$ Pa^{-1}.

Micro-electro-mechanical systems (MEMS) have seen remarkable growth in the last three decades, with numerous applications finding their way to commercialization: e.g., their use as pressure sensors, oscillators, and inertial measurement units.[1–3] Aiming for the era of Internet of Things (IoT), the next generation of MEMS devices requires the capability of multiple functionality integrated in a single device for big data collection and wider ranges of operating conditions for remote sensing applications.[4–6] MEMS applications for harsh environment monitoring fall within this trend, in which wide-bandgap materials such as III-Nitride, silicon carbide (SiC), and diamond-like carbon (DLC) are common choices due to their robustness and stability.[7,8]

Among these materials, aluminum nitride (AlN) thin films have been extensively developed and explored for high-frequency applications owing to their high surface phase velocity.[9,10] The material also offers a relatively high piezoelectricity when doped with scandium (Sc), which is suitable for MEMS oscillators.[11] This property also enables the development of surface acoustic wave (SAW) devices and radio frequency (RF) modules with improved performance. Another significant advantage of AlN is its use in HEMTs as a buffer layer to grow AlGaN/GaN stacking on Si, which offers exceptionally high electron mobility.[12,13] Nevertheless, AlN is generally grown on Si substrates, which exhibits a relatively large lattice mismatch and different thermal expansion.[14] This drawback typically causes problematic issues in electron mobility for HEMT devices and the acoustic loss in SAW applications.

Silicon carbide possesses a matching thermal expansion of coefficient and a comparable lattice constant with nitride piezoelectrics, thereby expected to provide better crystallinity for III-nitride films. Additionally, SiC piezoresistive material offers an ability to fabricate stress/stain sensing devices monolithically integrated into the same chip.[20,21] Recent studies have resulted in successful deposition of AlN

and GaN on a SiC substrate, with excellent performance compared to those grown on Si wafers.[15,16] The present template shows interesting potential for a wide range of applications including LEDs, SAW devices, and HEMTs.[17–19] However, as these III-nitride films were grown on bulk SiC substrates, the fabrication of MEMS devices is relatively challenging due to difficulties with defining micrometer size features in bulk SiC. Furthermore, in the previous reports, the SiC films only served as a buffer layer for III-nitride deposition, while their excellent electrical functions have been rarely utilized. The cubic crystalline SiC (3C-SiC) is the most favorable structure for layered SAW devices, as it can be readily grown on a Si substrate on a large scale. The 3C-SiC/Si wafer is also compatible with the existing industrial MEMS process, which is reflected in a large number of micro-devices fabricated out of this platform.[20,22]

Herein, we develop ScAlN/SiC/Si stacking films that offer different operating/sensing mechanisms generated by each deposited layer. The ScAlN/SiC bi-layers showed excellent electromechanical coupling, enabling the development of SAW devices with outstanding out-of-band rejection. The low-doped n-type 3C-SiC layer sandwiched between the ScAlN and Si substrate exhibits the highest reported piezoresistive effect in any 3C-SiC thin film that can be engineered through crystal orientation alignment for the maximum sensitivity of pressure/strain sensors. The fundamental piezoresistive coefficients of the low-doped n-type 3C-SiC thin film are calculated using the different crystallographic orientations and the applied stress directions. Leveraging the acoustic and piezoresistive properties in both ScAlN and SiC could open opportunities for multifunctional wide-bandgap systems (e.g., RF-MEMS and pressure sensors) that can be simply and compactly constructed in a single device.

Single crystal n-type 3C-SiC(100) thin films were grown to a thickness of 900 nm on the Si(100) substrate by the low pressure chemical vapor deposition (LPCVD) process at the temperature of 1250 °C. Alternating supply epitaxy (ASE) was employed to grow the single crystal 3C-SiC, and the precursors SiH_4 and C_3H_6 were employed as sources of Si and C atoms. The grown films exhibited unintentional n-type conductivity. The full details of the growth process can be found in Refs. 23 and 24. The deposition of ScAlN with 20% Sc on 3C-SiC/Si was carried out by the OEM group using the sputtering process. After the growth process, x-ray diffraction (XRD) analysis of the grown films was carried out to confirm the crystal structure followed by the rocking curve to analyze the crystalline quality. Figure 1(a) shows the XRD pattern of the ScAlN/3C-SiC/Si heterostructure in conventional θ-2θ scan mode. It can be observed that only the peaks corresponding to the (100) plane for the SiC thin film are present, which confirms that single crystal 3C-SiC(100) was grown on Si(100). For ScAlN, three different peaks are observed corresponding to its polycrystalline nature with the preferred orientation along the c-axis, i.e., ScAlN(002) peak. Figure 1(b) shows the rocking curve of the 3C-SiC(200) peak with the observed full width at half maximum (FWHM) value of 0.70°, which shows the good crystalline quality of the grown film. The rocking curve of the ScAlN (002) peak is given in Fig. 1(c), showing a FWHM value of 1.64°, which is a reasonably good value for a thin film grown by the sputtering method.

Figure 1(d) shows the transmission electron microscope (TEM) image of the ScAlN/3C-SiC interface, which shows that there are no boundaries in the 3C-SiC thin film and the only defects are stacking faults. The columnar growth of ScAlN is also evident from Fig. 1(e). The selected area electron diffraction (SAED) pattern in Fig. 1(d) reinforces the XRD results and confirms that the grown 3C-SiC thin film is single crystalline. Similarly, the SAED pattern of ScAlN confirms that the deposited thin film is polycrystalline as shown in Fig. 1(f). The conductance type and carrier concentration of the grown thin film

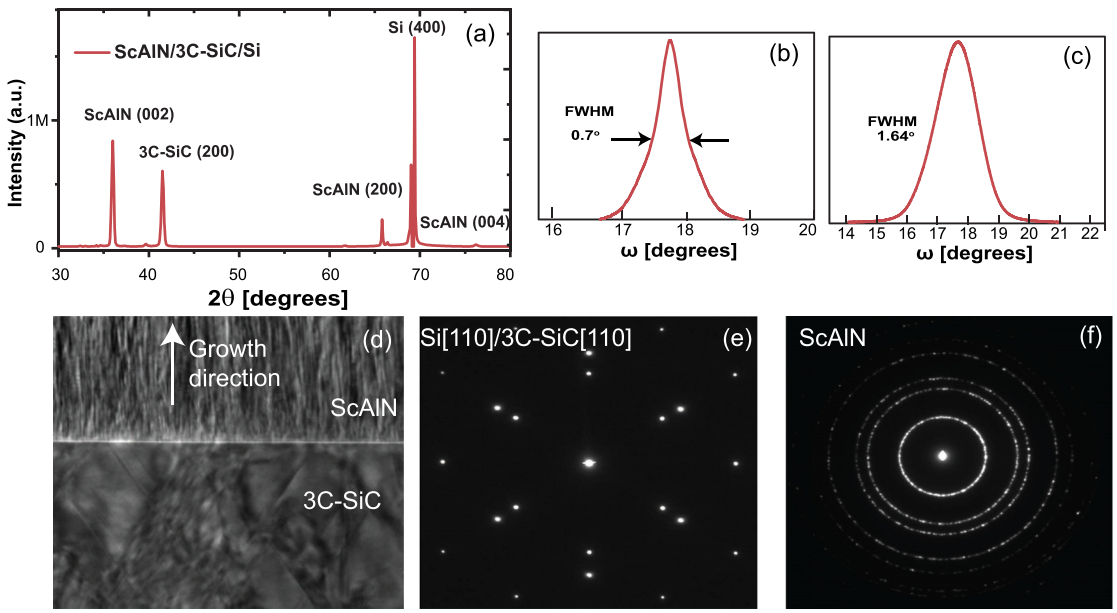

FIG. 1. (a) XRD pattern of the ScAlN/3C-SiC/Si heterostructure, (b) the rocking curve of the 3C-SiC(200) peak, (c) the rocking curve of the ScAlN(002) peak, (d) TEM cross-sectional image of the ScAlN/3C-SiC interface, (e) SAED pattern of 3C-SiC/Si in the [110] orientation, and (f) SAED pattern of the ScAlN thin film.

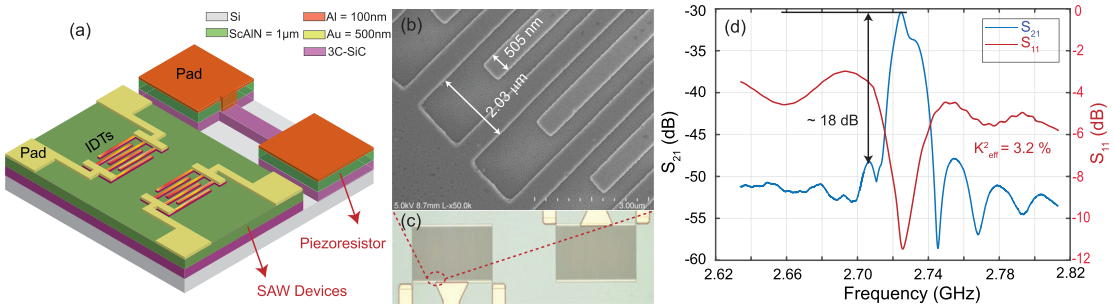

FIG. 2. (a) Schematic representation of the SAW device and a piezoresistor on a single substrate, (b) SEM image of the SAW IDTs, (c) microscope image of the SAW delay line, and (d) transmission and reflection spectra of the fabricated SAW device.

were obtained by hot probe measurements and then confirmed by Hall effect measurements. The carrier concentration of n-type single crystalline 3C-SiC(100) was found to be 5–8 × 10^{16} cm^{-3}. The carrier concentration of the Si substrates was 5 × 10^{14} cm^{-3}. The electrical resistivity of n-type 3C-SiC(100) was 17.4 Ω cm.

After the growth process, standard photolithography and dry etching processes were used to fabricate the SAW delay line devices along with fundamental resistors to characterize the piezoresistive effect [Fig. 2(a)]. Electron beam lithography was used to pattern interdigitated transducers (IDTs) with a finger width of 500 nm followed by Al metal lift-off, and ScAlN/3C-SiC etching was carried out by plasma etching. Figure 2(b) shows a scanning electron microscope (SEM) image of SAW IDTs, and a microscope image of the complete SAW delay line is shown in Fig. 2(c). The design parameters of the fabricated SAW devices are shown in Table I. A vector network analyzer was used to characterize the fabricated SAW devices in air and at room temperature. Prior to the measurements, a network analyzer was calibrated for on-chip probing using a short-open-load-through calibration standard. The measurements were taken using the standard G-S-G probe configuration. Figure 2(d) shows the measured transmission S_{21} and reflection S_{11} coefficients of the fabricated devices. It can be observed that the out-of-band rejection of the fabricated on-chip SAW device is very promising, which is 18 dB without using any impedance matching. The passband of the SAW device is approximately 20 MHz. The experimental K^2 values were measured using the following relation:[25]

$$K_{eff}^2 = \frac{\pi G(f_o)}{4NB(f_o)}, \tag{1}$$

where N is the number of finger pairs, $G(f_o)$ is the conductance, and $B(f_o)$ is the susceptance at resonant frequency f_o obtained using the Smith chart. The calculated electromechanical coupling is 3.2%, shown in the inset of Fig. 2(d). This value is much higher than the previously reported K^2 values in AlN and ScAlN, showing the potential of the ScAlN/3C-SiC/Si heterostructure stack for piezoelectric devices.

TABLE I. Design parameters for SAW delay lines.

IDT finger width (nm) = 500	Delay line length = 100λ
IDT pitch distance (nm) = 1000	IDT aperture = 100 μm
IDT number = 150	

A significant advantage in the stacking of different layers is the multifunctions that are provided by each layer. While ScAlN offers a marked piezoelectric property, the epitaxial SiC film not only provides a matching thermal expansion with ScAlN deposited on the top but also functions as a piezoresistive material. This is ideal for mechanical sensing applications where both dynamic and static modes are of interest. We investigated the strain sensing in the SiC films, by etching through the ScAlN film, and fabricated SiC resistors with Al contacts [Fig. 3(a)]. The strain effect was also investigated in different orientations by aligning SiC resistors in various crystallographic directions such as [100] and [110] to calculate the fundamental piezoresistive coefficients of the low-doped n-type 3C-SiC thin film.

Figure 3(b) shows the resistance change of the SiC films against strains induced by using a bending beam method.[20] Evidently, the resistance of n-type SiC exhibits a linear relationship with mechanical strains. It is also obvious that the change in the resistance of SiC depends on the crystal orientations. For instance, longitudinal [100] and [110] resistance decreased under tensile strain, while that of transverse [100] resistance shows an increase under the same mechanical loads. Based on these results, we estimated the gauge factors ($GF = \Delta R/R/\varepsilon$) in the SiC film to be –47, –23, and 18 with respect to longitudinal [100], longitudinal [110], and transverse [100]. Our result is higher than that reported by Shor *et al.*[26] and Eickhoff and Stutzmann.[27] It should be pointed out that the carrier concentration in our films falling within 10^{16} cm^{-3} to 10^{17} cm^{-3} is lower than those in the previous reports. The large gauge factor (GF) is reasonable and consistent with the theoretical model developed by Toriyama,[28] where decreasing the carrier concentrations will increase the piezoresistive coefficient.

As 3C-SiC is a cubic semiconductor, we employed the Euler matrix, to calculate the piezoresistive coefficient of the low-doped n-type 3C-SiC film,[29]

$$\begin{cases} GF_{[100],l} = \pi_{11} \times E_{SiC}, \\ GF_{[110],l} = \pi_{12} \times E_{SiC}, \\ GF_{[100],t} = -\frac{1}{2}(\pi_{11} - \pi_{12} - \pi_{44}) \times E_{SiC}. \end{cases} \tag{2}$$

Accordingly, the fundamental piezoresistive coefficients of a low-doped n-type 3C-SiC were found to be $\pi_{11} = (-14.5 \pm 1.3) \times 10^{-11}$ Pa^{-1},

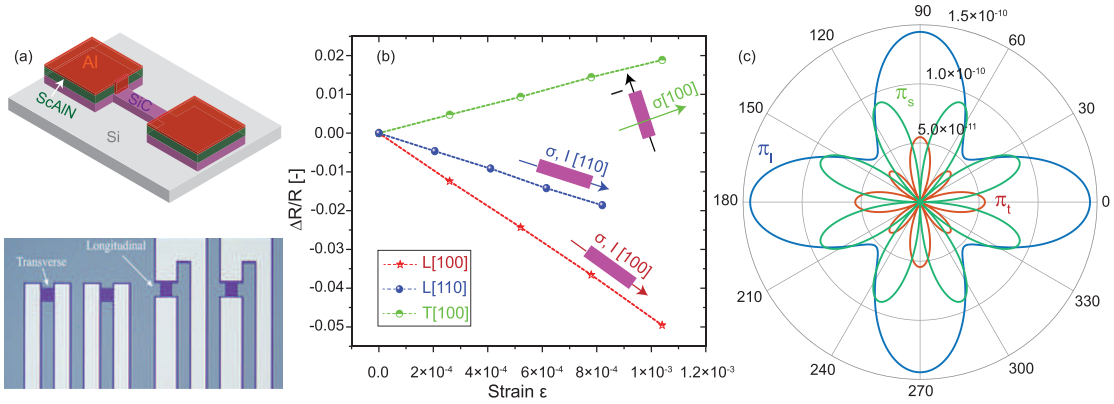

FIG. 3. Characterization of the piezoresistive effect in the low-doped 3C-SiC film; (a) concept and photograph of the testing samples, (b) the relationship between the applied strain and the change in SiC resistance aligning in different orientations, and (c) the piezoresistive coefficients π_l, π_t, and π_s calculated based on π_{11}, π_{12}, and π_{44}.

$\pi_{12} = (5.5\pm0.5) \times 10^{-11}$ Pa^{-1}, and $\pi_{44} = (-1.7\pm0.7) \times 10^{-11}$ Pa^{-1}, respectively. Using these coefficients, we estimated the longitudinal, transverse, and shear piezoresistive parameters in arbitrary orientation, Fig. 3. This graph serves as a guideline in the design of n-type 3C-SiC mechanical sensors integrated in a AlN material system.

We deposited high-quality ScAlN on an epitaxial SiC film, which was pre-grown on standard Si wafers. Both ScAlN and SiC films show excellent crystal quality, confirmed by XRD and TEM analyses. SAW devices developed out of the ScAlN films using the standard IDT configuration exhibit excellent out-of-ban rejection and electromechanical coupling, thanks to the superior piezoelectric properties of ScAlN and minimized acoustic loss by the support of the 3C-SiC thin film. Furthermore, the low-doped n-type 3C-SiC substrate provided an excellent piezoresistive effect with a large gauge factor of –47 in the [100] orientation. Combining the piezoelectricity in AlN and piezoresistance in SiC generates multi-functionality in wide-bandgap semiconductor-based devices.

The authors acknowledge the technical support of the staff at the Lurie Nanofabrication Facility (LNF) of the University of Michigan, the Queensland Microtechnology Facility, which is part of the Queensland node (Griffith University) of the Australian National Fabrication Facility, for 3C-SiC material growth and OEM group for ScAlN deposition. This project was supported by the Army Research Office (ARO), Defense Advanced Research Projects Agency (DARPA), and National Aeronautics and Space Administration (NASA) SMD office. This work was also partially funded by the Griffith University's New Researcher Grants and Australian Research Council under No. DE200100238.

The data that support the findings of this study are available within this article.

REFERENCES

[1]K. Totsu, M. Moriyama, and M. Esashi, Nat. Electron. **2**, 134–136 (2019).
[2]X. L. Feng, C. J. White, A. Hajimiri, and M. L. Roukes, Nat. Nanotechnol. **3**(6), 342–346 (2008).
[3]D. S. Breed, "Inertial measurement unit for aircraft," U.S. patent 7962285 (26 June 2008).
[4]M. A. Feki, F. Kawsar, M. Boussard, and L. Trappeniers, Computer **46**(2), 24–25 (2013).
[5]M. M. Izaguirre, C. A. Mazza, M. Biondini, T. T. Baldwin, and C. L. Ballare, Proc. Natl. Acad. Sci. **103**(18), 1170–7174 (2006).
[6]V. Balakrishnan, H.-P. Phan, T. Dinh, D. V. Dao, and N.-T. Nguyen, Sensors **17**(9), 2061 (2017).
[7]H.-P. Phan, D. V. Dao, K. Nakamura, S. Dimitrijev, and N.-T. Nguyen, J. Microelectromech. Syst. **24**(6), 1663–1677 (2015).
[8]A. Krishna, A. Raj, N. Hatui, S. Keller, and U. Mishra, Appl. Phys. Lett. **115**, 172105 (2019).
[9]S. Strite and H. Morkoc, J. Vac. Sci. Technol., B **10**(4), 1237–1266 (1992).
[10]A. Qamar, M. Jafari, and M. Rais-Zadeh, IEEE Electron Device Lett. **39**(12), 1916–1919 (2018); A. Qamar, S. Sherrit, X. Zheng, J. Lee, P. X. Feng, and M. Rais-Zadeh, J. Microelectromech. Syst. **28**(4), 619–627 (2019).
[11]K. Hashimoto, S. Sato, A. Teshigahara, T. Nakamura, and K. Kano, IEEE Trans. Ultrason. Ferroelectr. Freq. Control **60**(3), 637–642 (2013).
[12]A. S. Yalamarthy, M. M. Rojo, A. Bruefach, D. Boone, K. M. Dowling, P. F. Satterthwaite, D. Goldhaber-Gordon, E. Pop, and D. G. Senesky, Nano Lettt. **19**(6), 3770–3776 (2019).
[13]A. S. Yalamarthy, H. So, M. M. Rojo, A. J. Suria, X. Xu, E. Pop, and D. G. Senesky, Adv. Funct. Mater. **28**(22), 1870152 (2018).
[14]A. Tanaka, W. Choi, R. Chen, and S. A. Dayeh, Adv. Mater. **29**(38), 1702557 (2017).
[15]J. Lemettinen, N. Chowdhury, H. Okumura, I. Kim, S. Suihkonen, and T. Palacios, IEEE Electron Device Lett. **40**(8), 1245–1248 (2019).
[16]N. Onojima, J. Suda, T. Kimoto, and H. Matsunami, Appl. Phys. Lett. **83**(25), 5208–5210 (2003).
[17]D. Massoubre, L. Wang, L. Hold, A. Fernandes, J. Chai, S. Dimitrijev, and A. Iacopi, Sci. Rep. **5**(1), 1–8 (2015).
[18]W. C. Kao, W. H. Lee, S. H. Yi, T. H. Shen, H. C. Lin, and M. J. Chen, RSC Adv. **9**(22), 12226–12231 (2019).
[19]R. Aubry, J. C. Jacquet, M. Oualli, O. Patard, S. Piotrowicz, E. Chartier, N. Michel, L. T. Xuan, D. Lancereau, C. Potier, and M. Magis, IEEE Electron Device Lett. **37**(5), 629–632 (2016).
[20]H.-P. Phan, D. V. Dao, P. Tanner, L. Wang, N.-T. Nguyen, Y. Zhu, and S. Dimitrijev, Appl. Phys. Lett. **104**(11), 111905 (2014).
[21]A. Qamar, H.-P. Phan, J. Han, P. Tanner, T. Dinh, L. Wang, S. Dimitrijev, and D. V. Dao, Mater. Chem. C **3**(34), 8804–8809 (2015).
[22]A. Qamar, P. Tanner, D. V. Dao, H. Phan, and T. Dinh, IEEE Electron Device Lett. **35**(12), 1293–1295 (2014); A. Qamar *et al.*, *ibid.* **36**(7), 708–710 (2015).
[23]L. Wang, S. Dimitrijev, J. Han, P. Tanner, A. Iacopi, and L. Hold, J. Cryst. Growth **329**(1), 67 (2011).
[24]L. Wang, A. Iacopi, S. Dimitrijev, G. Walker, A. Fernandes, L. Hold, and J. Chaia, Thin Solid Films **564**, 39 (2014).

[25]O. Elmazria, V. Mortet, M. E. Hakiki, M. Nesladek, and P. Alnot, IEEE Trans. Ultrason. Ferroelectr. Freq. Control **50**(6), 710–715 (2003).
[26]J. S. Shor, D. Goldstein, and A. D. Kurtz, IEEE Trans. Electron Devices **40**(6), 1093–1099 (1993).
[27]M. Eickhoff and M. Stutzmann, J. Appl. Phys. **96**(5), 2878 (2004).
[28]T. Toriyama and S. Sugiyama, in Proceedings of International Symposium on Micromechatronics and Human Science (MHS) (2000), pp. 175–180.
[29]Y. Kanda, Sens. Actuators, A **28**, 83 (1991).